

The Validation of Fe Modeling of Orthogonal Turning Process Using Cowper–Symonds Material Behavior Law

Virginija GYLIENE, Vytautas OSTASEVICIUS

*Kaunas University of Technology (KTU), Department of Engineering Design
Faculty of Mechanical Engineering and Mechatronics
Kęstučio St. 27, LT-44312 Kaunas, Lithuania; e-mail: virginija.gyliene@ktu.lt*

The article contains a literature review, experimental results, and a Finite Element Model (FEM) composition. Orthogonal turning tests were executed in the range of cutting speeds and feed rate, after every test chip was collected.

Further investigation was done using FE model validation and experimentation, which uses results of the experimental zone in which the built-up edge did not form and the cutting itself is of even plastic deformation.

The essence of this research is that the adequacy of the composed FE model to the real physical process should conform not only to the evaluation of cutting forces, but also to the evaluation of chip form, that is, segmentation frequency.

Key words: orthogonal cutting, FE modelling, deformation rate, chip segmentation.

1. INTRODUCTION

Material removal by cutting remains one of the most common technological processes for producing complex and high-precision components (taking into account the coefficient of component complexity [1]). Research of cutting processes may be subdivided into the following fields: tribology, cutting tools and coatings, environment-friendly machining, vibration phenomena in cutting, machinability, process optimization, component quality, mechatronic problems, improvement of process efficiency, and diagnostics and computer systems [2].

The aforementioned classification demonstrates the multitude of mutually interrelated research fields that are important in studying different cutting processes. The machining research community is particularly interested in the chip formation processes, which deals with material deformation during cutting, including the influence of deformable material on the tool. Cutting forces, temperature, tool wear, friction between tool and chip, machining power, and surface quality are all dependent on chip formation [3]. These physical effects are studied

by means of numerical methods. Mathematical modeling of the associated technological processes involves such important procedures as task description and verification of numerical solution against experimental values obtained during investigation of actual physical processes.

Modeling of cutting processes is predominantly performed by means of simplified approaches, which have been already employed by Tresca and Mallock in their initial research works [1]. One group of researchers has used of finite element procedures for studying the influence of the cutting edge on the cutting process [4–7]. Meanwhile, another group of scientists has focused on investigation of the chip formation mechanism with consideration of aspects of tool durability [8–10]. These studies require physically validated finite element models, which are commonly verified by using experimentally determined cutting forces; though, there is an increasing trend to pay more research attention to the geometrical configuration of the removed chip [11]. Author ZHANG *et al.* [12] proposes an FE model with an improved friction model. Further investigation [12] presents the impact of cutting speed to the morphology of the cutting chip. On the other hand, in cases when numerical and experimental results are compared, the reliability of data used for FEM validation must be ensured too.

A wider scope of investigated parameters and effects in cutting are promoted by increasing the application of explicit numerical schemes during finite element analysis. Engineering analysis software with implemented explicit approaches employ more efficient algorithms for solution of contact and other dynamic problems, thereby reducing required computational time that is directly proportional to size of finite elements [13]. Machining with “low” and “high” cutting velocities leads to increased material deformation rates that may vary in the range of 10^3 – 10^6 s⁻¹ [9]. Thus, characterization of material flow in these conditions is a highly sophisticated problem. Some of the researchers use high-velocity compression and Hopkinson tests for evaluation of material behavior under large strain rates, while others rely on application of experimental results of orthogonal turning in conjunction with finite element analysis [14].

This paper presents experimental results that have obtained in a wide range of cutting velocities with the purpose to avoid formation of built-up edge zones. This experimental research consisted in measurement of cutting forces and characterization of accumulated chips. The actual material characteristics had established by means of tensile testing. For further FE analysis plastic kinematic material deformation model was suited to model isotropic and kinematic hardening plasticity with option of including rate effects. A finite element model had developed for investigation of orthogonal cutting process by employing a tool with a sharp cutting edge. Literature survey indicates that a tool is considered to have a “sharp” edge when its sharpness value is within the limits of 0–31 μm [15–17]. A measurement device was used to determine sharpness of tool edge by

means of method of tangential lines [18, 19]. As it will be reasoned later in this paper, one parameter for FE model validation is not sufficient.

2. EXPERIMENTAL INVESTIGATION

2.1. Turning Experiments

The experimental research was performed for the case of orthogonal cutting with the aim of measuring the generated cutting forces and determining the change of chip form ($F = f(V_c)$, $F = f(p)$). The experimental setup and geometrical approach for FE model composition is presented in Fig. 1.

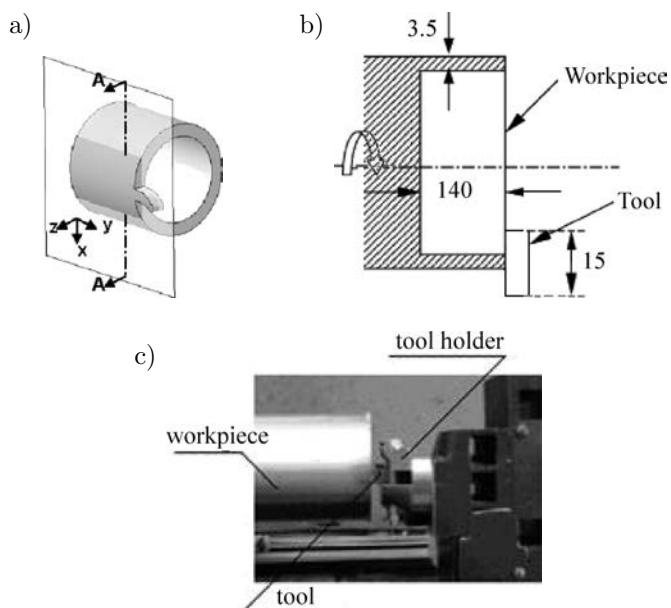


FIG. 1. Schematics of orthogonal turning experiment setup: a) cross-sectional workpiece for FEM (adopted from [20]); b) workpiece dimensions; c) experimental setup.

A special “tube-type” work-piece was fabricated to conduct orthogonal cutting experiments. This type of work-piece is not so commonly used as, for example, disks or toothed shafts. However, the main benefit of the “tube-type” work-piece is that its diameter remains unmodified during orthogonal cutting.

The experiments were carried out by using carbide tool T5K10 (85% WC, 6% TiC, 9% Co), which rake and clearance angles are respectively equal to $\gamma = 0^\circ$, $\alpha = 20^\circ$. The tool was mounted into a special holder, with strain-gauge dynamometer mounted underneath, thereby enabling measuring of tangential (F_T) and radial (F_R) cutting force components. Dynamometer signals were amplified and subsequently processed by means of Picolog software.

Generated chips were collected after each test sequence (each experiment was repeated 3 times) when the workpiece was machined in the range of cutting velocities of 0.42–3.6 m/s and feed rate (or so-called depth of cut, which is the particularity of orthogonal turning process) $p = 0.05 \div 0.1$ mm/rot.

Figure 2a provides the distribution of measured cutting forces, which variation character indicates specific physical phenomena. The presented relationships reveal three distinct zones:

- 1 – zone of low cutting velocities (up to 0.72 m/s), which was characterized by force increase or decrease due to discontinuous formation of chips as well as plastic irregularities.
- 2 – zone of velocities from 0.72 m/s (250 rot/min) till 1.81 m/s (630 rot/min), which was not an optimal cutting condition from the technological point of view because of rapid increase of cutting forces. Figure 2a indicates that maximal values of the tangential force depends on the feed rate, i.e. under lower feed value, maximal tangential force is reached under larger cutting velocities and *vice versa*.
- 3 – zone of velocities up from 1.88 m/s (*in these particular experimental study*), which was characterized by continuous plastic deformation (*without formation of built-up edge*) and settled/decreasing cutting forces.

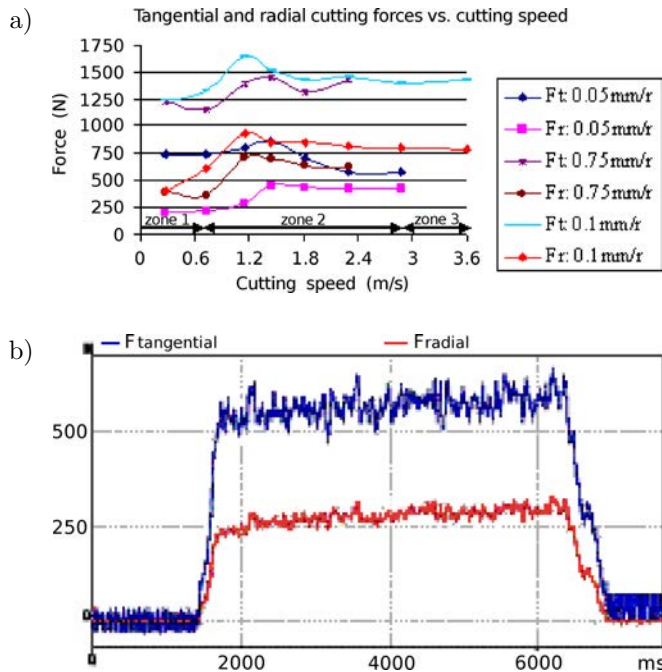


FIG. 2. Cutting forces distribution, assuming cutting speed and cutting feed rate: a) all performed orthogonal tests results; b) measured forces from test: 0.05 mm/rot and 2.88 m/s.

After the cutting experiments, the microsections were prepared and used to determine chip thickness and segmentation frequency. Experimental results that are characteristic to the 3rd zone were subsequently applied for finite element modeling. The chips form of the so-called 3rd zone of cutting was estimated. According to results, presented in Fig. 2a the cutting conditions ($V_c = 2.88$ m/s, $p = 0.05$ mm/rot) were taken for future FE modeling. Figure 3 presents chip form change according to cutting depth. In order to take the pictures, a Nikon Eclipse LV150 microscope was used equipped with an Infinity 1 camera connected to a computer.

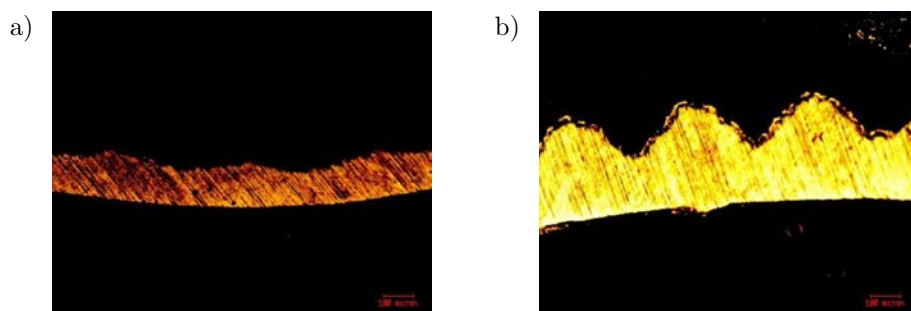


FIG. 3. Chips from 3rd cutting zone according to cutting speed and cutting feed:
 a) $V_c = 2.88$ m/s, $p = 0.05$ mm/rot; b) $V_c = 2.88$ m/s, $p = 0.1$ mm/rot.

To determine the chip segmentation frequency the geometric parameters, as the width of repeated segments were measured. Assuming the shape of chip for cutting speed in the 3rd zone it was defined, that segmentation frequency was about 6.1 kHz and 6.7 kHz respectively for feed 0.05 mm/rot and 0.1 mm/rot.

2.2. Determination of mechanical properties of material

Actual mechanical properties of 35-grade steel (0.32–0.4% C) were determined by tensile testing in order to obtain reliable input data for the developed FE model. During each test the average results of the thickness and load were obtained and approximated to determine the real characteristics of the materials. Figure 4 presents the dependence of the real tension to the deformation.

The material strengthening effect is determined by the material hardness [21]. Rockwell hardness testing yielded the value of 35 HRC for the tested steel material. It is known that cutting of steels of such or similar hardness under both low and high velocities results in formation of continuous chip (*when the feed rate is small*) [22].

Table 1 provides the determined mechanical properties of 35 grade steel, which were applied for construction of deformation law of the material in the finite element model.

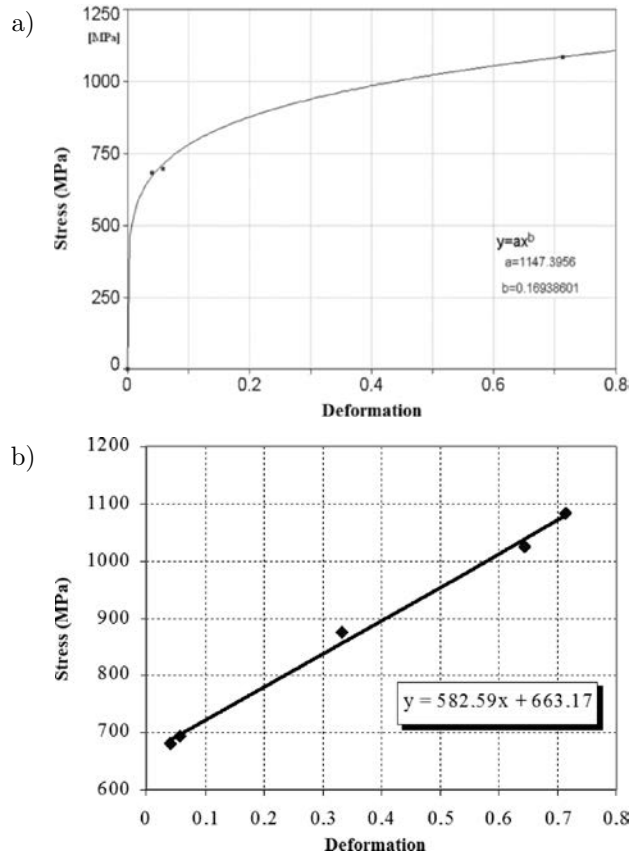


FIG. 4. The dependence of the real stress to the deformation: a) dependence between the stresses and deformation during the testing; b) schematized dependence between the stresses and deformation.

Table 1. Material properties of 35 grade steel.

Characteristics	Defined by Tensile Test	Used in FEM Cowper–Symonds law
Density [kg/m^3]	7800	+
Young modulus [GPa]	200	+
Poisson index [-]	0.29	+
Yield stress [MPa]	663	+
Strength limit [MPa]	698	-
Failure strain [-]	0.72	+
Tangential modulus [MPa]	582.6	+
Hardening index [-]	0.169	-
Cowper–Symonds constants C [s^{-1}]; P [-]	-	220; 5
Kinematic–isotropic material hardening constants [-]	-	0–1

3. NUMERICAL SIMULATION OF ORTHOGONAL TURNING PROCESS

3.1. Description of the numerical model

LS-DYNA/Explicit FE code was employed for modeling purposes. For 3D modeling and nonlinear dynamic simulations a solid element SOLID164 was used, which consists of 8 nodes with three degrees of freedom at each node in X , Y , Z directions. Both coarse and fine meshing was used in the FE model depending on deformation intensity in the considered zone. The number of finite elements was appropriately reduced by diminishing the size of the FE elements only in the area of contact interaction, which usually requires an extremely fine mesh resulting in huge computational efforts. Figure 5 presents the developed FE model that was divided into several zones, which was accomplished by means of commands *lesize*, *nmgall* of Ansys that was used as a pre-processor environment in this research work. Parameters of the model are as follows: rake angle $\gamma = 0^\circ$, clearance angle $\alpha = 20^\circ$, edge sharpness $r = 13 \mu\text{m}$, cutting depth $p = 0.05 \text{ mm}$. From the results presented in Fig. 5 it was found that the mesh density (8 elements per layer to cut – depth of cut) is sufficient for the accuracy

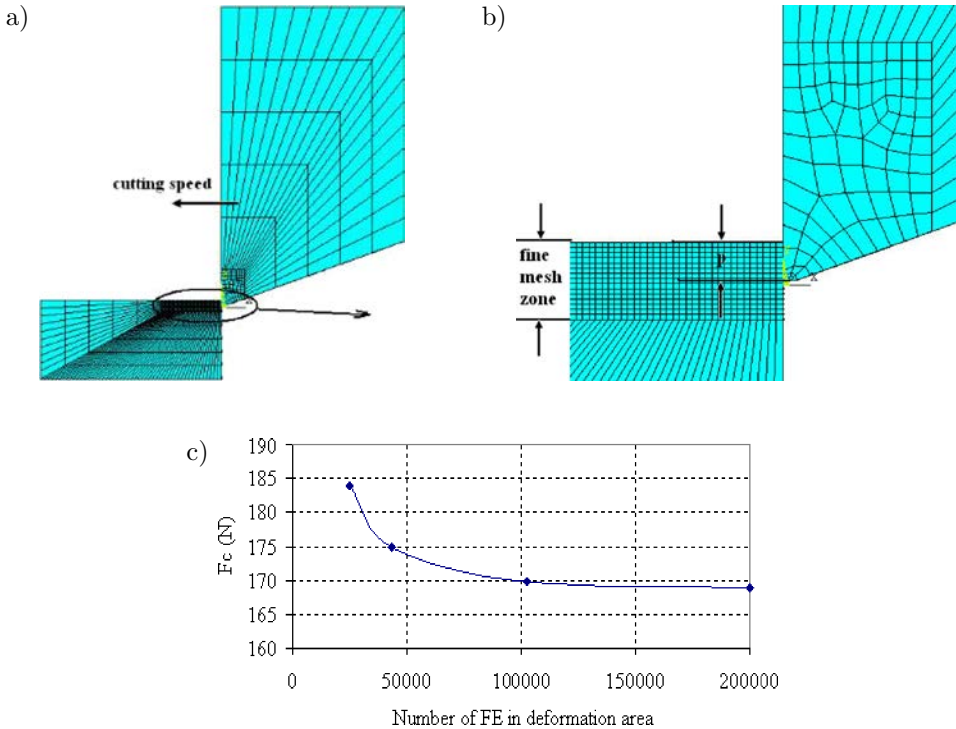


FIG. 5. Finite element model: a) full FE model; b) FE model in detail; c) definition of mesh size (*test without dynamic characteristic*).

according to mesh size. Finally, for time cost saving and the need of small time step the area to remove was diminished to 0.05×0.05 mm (workpiece: 28980 elements). Boundary conditions of the FE model were as follows. The workpiece was constrained in all six DOFs. Load of type $U = f(t)$ was imposed on the tool with the purpose to simulate cutting motion with respect to cutting velocity. Numerical FE model of cutting process was formed evaluating contact between interacting bodies (*deformable body – rigid body*). In *LS-DYNA* package contact interaction between two bodies was formulated using “master–slave” methodology and penalty method. The friction in the contact, in *LS-DYNA* package, is expressed in the following way [23]:

$$(3.1) \quad f = f_s + (f_s - f_d)e^{-DC|V_{\text{rel}}|},$$

here f_d – dynamic coefficient of friction; f_s – static coefficient of friction; DC – exponential decay coefficient; V_{rel} – relative velocity.

A literature survey [24–27] indicates that in the case of our cutting experiments ($p = 0.05$ mm, $V_c = 2.88$ m/s) the coefficient of friction may vary in the range of $\mu = 0.43 \div 0.72$. A value of 0.5 was used for determination of dynamic constants.

The problem as cutting process simulation is classified as high velocity contact–impact interaction problem. So, elastic–plastic material model with kinematic–isotropic hardening was chosen. The strain rate is accounted for by using the Cowper and Symonds model which scales the yield stress by strain rate dependent factor [23]:

$$(3.2) \quad \sigma_Y = \left[1 + \left(\frac{\dot{\varepsilon}}{C} \right)^{1/P} \right] (\sigma_{Y0} + \beta E_P \varepsilon_{\text{eff}}^P),$$

where σ_Y , σ_{Y0} – yield stress limits of the material defined with and without the influence of strain rate $\dot{\varepsilon}$; P and C are user defined input constants.

The current radius of the yield surface σ_Y is the sum of the initial yield strength σ_{Y0} , plus the growth $\beta E_P \varepsilon_{\text{eff}}^P$, where E_P is the plastic hardening modulus:

$$(3.3) \quad E_P = \frac{E_t E}{E - E_t},$$

where E_t – tangential modulus (MPa), $\varepsilon_{\text{eff}}^P$ – effective plastic strain, β – constant, defining kinematic ($\beta = 0$), isotropic ($\beta = 1$) or kinematic–isotropic hardening ($0 < \beta < 1$).

On the basis of Eq. (3.2), it is clear that the static and dynamic yield stress ratio depends on deformation speed. Values P and C in relation (3.2) and the

kind of hardening hypothesis (kinematical, isotropic or the combination of two) can be assumed as parameters the values of which need to be determined in order to achieve the adequacy of simulation results to reality [28]. Tangent modulus needed for the simulation was defined by tensile tests. All material parameters defined by tensile test and parameters used in material model are listed in Table 1.

Time step size control measures can be regarded as common practice in explicit dynamics calculation where very large strains [9] are expected. They can be interpreted as a “safety catch”, activated in order to cope with the elements that lose their physical meaning because of excessive straining [28]. During impact–contact simulation the elements of the material to remove (the chip) are highly deformed and require to decrease the time integration step. The time integration step in explicit integration techniques cannot be greater than the least time duration during which the elastic longitudinal wave passes the smallest element of the structure [28]. As the simulation goes on, the time step tends to become shorter and solution may never end. So, in the presented work, a time step size control technique implemented in LS-DYNA was used as deletion of solid elements too degenerated. The material failure criterion was set as failure strain.

At the initial stage of simulations deformation rate was ignored. Dynamic constants C and P of Cowper–Symonds function were not used during modeling of orthogonal cutting process. Chip separation constitutes one of the most important parts of chip removal process. At the initial stage, the failure strain was set to 0.8 (*similar to the static value obtained from tensile tests*). Some researchers claim that the magnitude of the fracture deformation does not affect simulation results [8]. It was demonstrated that when neglecting deformation rate (*i.e. without artificial enlarging of yield limit*), the maximal achieved value of cutting force is equal to 170 N, which is 3.4 times smaller than the experimental value.

Thus, taking into consideration that in the course of cutting process the material was subjected both to temperature effect and influences arising from high deformation rate, the actual failure strain value maybe be 1.16–1.75 times larger than its static equivalent [29]. Finally, the set of simulations with different failure strain (0.8; 1.0; 1.2; 1.4) were performed. Figures 6a and 6b presents the FE modeling results, assuming failure strain at the initial stage of chip formation.

It was defined, that failure strain influence the shape of chip in the initial cutting stage, the distribution of strain, shear localization and distribution (according to 1st and 2nd shear in cutting zone) and finally cutting force. Failure strain non influences shear formation (this is the case study with 0 rake angle).

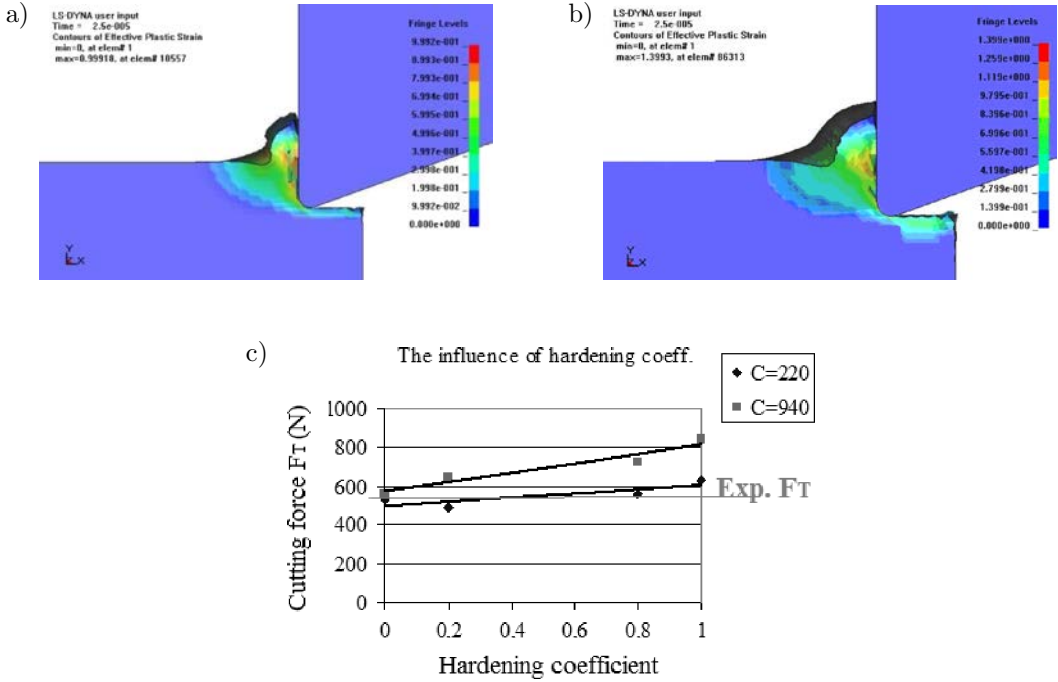


FIG. 6. Chip formation: a) $f_{st}=1.0, t=0.025$ ms; b) $f_{st}=1.4, t=0.025$ ms.

Figure 6c presents the cutting force variation according to Cowper–Symonds constants and material hardening coefficients ($C = 220 \text{ s}^{-1}, P = 5$ and $C = 940 \text{ s}^{-1}, P = 3.5; f_{st} = 0.8$). The choice of the type of hardening law may influence the results dramatically. Both series of simulations the combination with hardening coefficient which corresponds correctly (2.1%) with experimental results ($F_t = 572 \text{ N}$), when using kinematic hardening with constants $C = 940 \text{ s}^{-1}, P = 3.5$. The same results are achieved using kinematic–isotropic hardening ($\beta = 0.8$) with constants $C = 220 \text{ s}^{-1}, P = 5$. Consequently, it is here that another precision of chip formation is needed. The chip form, specifically the chip segmentation frequency, is defined from chip geometrical elements and was introduced to the precise FE model.

According to the authors [28], the choice of dynamic constants can not be an “accidental mix”; and here the ambiguity is possible while selecting Cowper–Symonds (C and P) constants. Both of them belong to Cowper–Symonds yield limit scaling model and to some extent are able to compensate each other [28]. For that reason as presented in Fig. 6c more attention is paid to FE model adjustment. It is suggested to check not only one experiment output parameter with numerical results. Figure 7 presents modelling results with extreme material hardening constants.

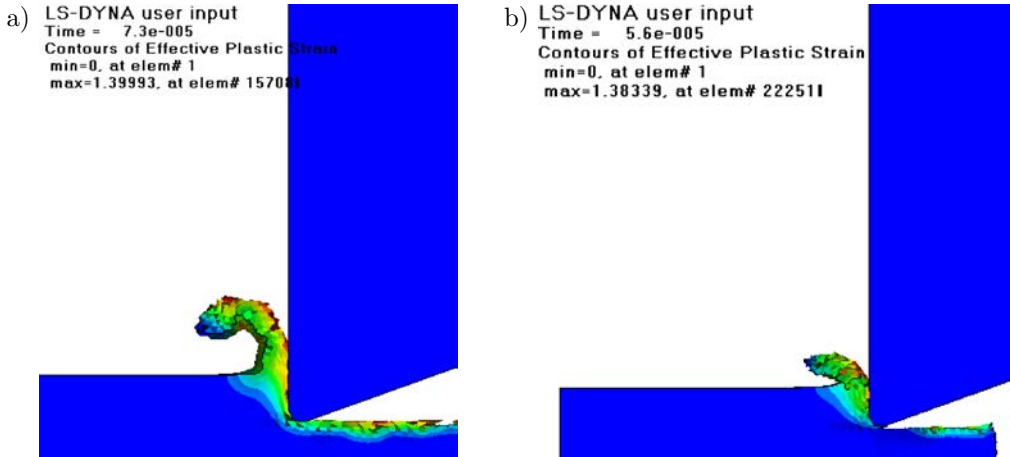


FIG. 7. Chip formation, according to material kinematic and isotropic hardening: a) chip formation with kinematic hardening: continuous chip with formed segments ($C = 220 \text{ s}^{-1}$, $P = 5$, $\beta = 0$, $f_{st} = 1.4$), $F_{t \text{ calc}} = 529 \text{ N}$ (7.6% less experimental value); b) chip formation with isotropic hardening: failure of chip ($C = 220 \text{ s}^{-1}$, $P = 5$, $\beta = 1$, $f_{st} = 1.4$), $F_{t \text{ calc}} = 640 \text{ N}$ (11.8% more experimental value).

Performed orthogonal turning simulations in the range of material kinematic, kinematic–isotropic, isotropic hardening presented chip formation from continuous segmented (or laminar) to chip failure. Idem, cutting force increase going to use kinematic–isotropic and isotropic hardening (Fig. 6c).

Finally, it was tested the set of Cowper–Symonds constants and material hardening constant which matches up to experimental results. Figure 8 presents the results of simulation with material constants: $C = 940 \text{ s}^{-1}$, $P = 3.5$ ($\beta = 0$) and $C = 220 \text{ s}^{-1}$, $P = 5$ ($\beta = 0.8$) and $f_{st} = 1.4$.

As it is presented in Fig. 8a kinematic hardening perform much more regular chip comparing with isotropic material hardening. However, some authors [28], using Cowper–Symonds material behavior law in ballistics proposes to use isotropic hardening if thermal phenomenon appears. The main application of the developed FE model can be the field of high-speed machining (HSM) processes. Because, only 17% of primary heat zone flows into the workpiece [30].

As it was demonstrated the material behavior law, assuming constants, defining deformation rate can't be used only by validation numerical model with only on numerical model output parameter. However, chip form, especially chip segmentation frequency was chosen to validate FE model. It was defined finally, that performed FE model with failure strain 1.4 (kinematic or isotropic hardening) does not match the segmentation frequency of chip (with a difference of least four times). Though it was stated, what Cowper–Symonds material behavior law with kinematic hardening numerically generate perfectly continuous

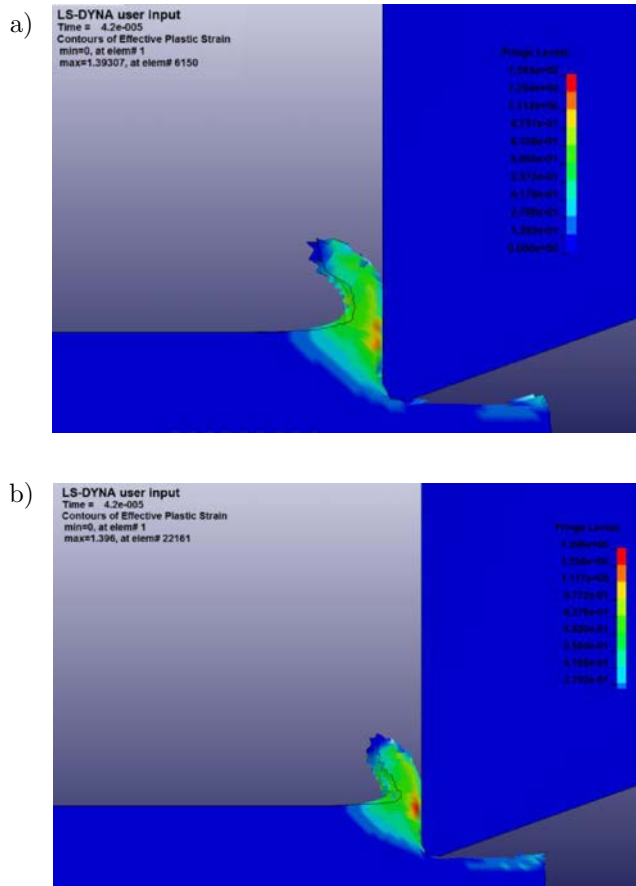


FIG. 8. Chip formation, according to material kinematic and isotropic hardening: a) chip formation with kinematic hardening: continuous chip ($C = 940 \text{ s}^{-1}$, $P = 3.5$, $\beta = 0$, $f_{st} = 1.4$), $F_{t \text{ calc}} = 588 \text{ N}$ (+2.7% experimental value); b) chip formation with kinematic-isotropic hardening: ($C = 220 \text{ s}^{-1}$, $P = 5$, $\beta = 1$, $f_{st} = 1.4$), $F_{t \text{ calc}} = 644 \text{ N}$ (+12% experimental value).

chip. Thus, there it can be stated that the best application of composed FE numerical model can be the generated chip load on cutting tool.

4. CONCLUSIONS AND PERSPECTIVES

The large experimental area of turning tests provided the experimental case (*uniform plastic deformation, no built-up formation, no resonance phenomenon*) for FE modelling of orthogonal cutting process. The analysis presented showed the ambiguity of the use of Cowper–Symonds material behavior law in modelling of cutting process.

First, both isotropic and kinematic material hardening presents “desirable” numerical results, according to the cutting force. Secondly, the final adjustment of numerical model of the cutting process can be done only by checking the chip form generation.

There it can be stated that the best application of composed FE numerical model can be the generated chip load on cutting tool.

Assuming chip form for further FE modelling elastic–plastic material model with kinematic (or kinematic–isotropic) hardening should be proposed.

ACKNOWLEDGMENTS

Research support was provided by Research Council of Lithuania through the project No. MIP–113/2010 (VibroCut).

REFERENCES

1. CHILDS T., MAEKAWA K., OBIKAWA T., YAMANE Y., *Metal machining. Theory and applications*, London, 2000.
2. ZATARAIN M., *Manufacturing technologies: current researching trends*, 5th International Conference on High Speed Machining, pp. 1–38, Metz, France, 2006.
3. XIE J.Q., BAYOUMI A.E., ZBIB H.M., *FEA modeling and simulation of shear localized chip formation in metal cutting*, Int. J. of Machine Tools & Manufacture, **38**, 1067–1087, 1998.
4. RECH J., YEN Y.C., HAMDI H., ALTAN T., BOUZAKIS K.D., *Influence of cutting edge radius of coated tool in orthogonal cutting of alloy steel*, Materials Processing and Design: Modeling, Simulation and Applications – NUMIFORM 2004 – Proceedings of the 8th International Conference on Numerical Methods in Industrial Forming Processes, AIP Conference Proceedings, Volume 712, pp. 1402–1407, 2004.
5. YEN Y.C., JAIN A., ALTAN T., *A finite element analysis of orthogonal machining using different tool edge geometries*, Journal of Materials Processing Technology, **146**, 1, 72–81, 2004.
6. ASTAKHOV V.P., *A treatise on material characterization in the metal cutting process. Part 2: Cutting as the fracture of workpiece material*, J. of Materials Processing Technology, **96**, 34–41, 1999.
7. BOUZAKIS K.D., MICHAILIDIS N., SKORDARIS G., KOMBOGIANNIS S., HADJIYIANNIS S., EFSTATHIOU K., ERKENS G., RAMBADT S., WIRTH I., *Effect of cutting edge radius and its manufacturing procedure, on the milling performance of PVD coated cemented carbide inserts*, Annals of the CIRP, **51**, 61–64, 2002.
8. HAMMAN J.C., GROLEAU V., LE MAITRE F., *Machinability improvement of steels at high cutting speeds – study of tool/work material interaction*, Annals of the CIRP, **45**, 87–92, 1996.
9. GUO Y.B., *An integral method to determine the mechanical behavior of materials in metal cutting*, J. of Materials Processing Technology, **142**, 72–81, 2003.

10. GUO Y.B., LIU C.R., *Residual stress formation mechanism and its control by sequential cuts*, Transactions of Namri/ASME, **28**, 179–184, 2000.
11. BAKER M., *Finite element investigation of the flow stress dependence of chip formation*, J. of Materials Processing Technology, **167**, 1, 1–13, 2005.
12. ZHANG Y.C., MABROUKI T., NELIAS D., GONG Y.D., *Chip formation in orthogonal cutting considering interface limiting shear stress and damage evolution based on fracture energy approach*, Finite Elem. Anal. Des., **47**, 7, 850–863, 2011.
13. GARCIA ARANDA M.L., *Etude thermo-mécanique et modélisation numérique de l'emboutissage à chaud de l'Usibor 1500* [in French], PhD-Thesis, Ecole des Mines de Paris, 2004.
14. CHIGURUPATI P., JINN J.T., OH J.Y., YIN Y., ZHANG H., WU W.T., *Advances in Machining Process Modeling*, AIP Conference Proceedings, **712**, 2004.
15. HUA J., SHIVRUPI R., CHENG X., BEDEKAR V., MATSUMOTO Y., HASCHIMOTO F., WATKINS T.R., *Effect of feed rate, workpiece hardness and cutting edge on subsurface residual stress in the hard turning of bearing steel using chamfer + hone cutting edge geometry*, Materials Science and Engineering, **394**, 238–248, 2005.
16. ARRAZOLA P.J., DONE U., VILLAR J.A., MARYA S., *Finite element modelling: a qualitative tool to study high speed machining*, 5th International Conference on High Speed Machining, pp. 239–246, Metz, France, 2006.
17. FILONENKO S.N., *Metal cutting* [in Russian], Kiev, 1969.
18. SKIEDRAITE I., KUWAHARA M., FUJI H., *Contact tangential method for measurement of tool geometry* [in Japanese], Patent No 37163310, Japan.
19. SKIEDRAITE I., SLEINIUTE V., *Measurement of tool – edge geometry*, Mechanics, **6**, 50, 64–67, 2004.
20. RACZY A., ALTENHOF W.J., ALPAS A.T., *An Eulerian Finite Element Model of the Metal Cutting Process*, Proceedings of 8th international Ls–Dyna Users conference, 11–25, 2004.
21. BAKER M., ROSLER J., SIEMERS C., *A finite element model of high speed metal cutting with adiabatic shearing*, Computers & Structures, **80**, 495–513, 2002.
22. FALLBOHMER P., RODRIGUEZ C.A., OZEL T., ALTAN T., *High-speed machining of cast iron and alloy steels for die and mould manufacturing*, J. of Materials Processing Technology, **98**, 104–115, 2000.
23. *LS-DYNA Theoretical manual*, Livermore Software Technology Corporation, 1998.
24. SHAW MILTON C., *Metal cutting principles*, Oxford, 1997.
25. GRANOVSKI G.I., GRANOVSKI V.G., *Metal cutting* [in Russian], Moscow, 1985.
26. MOLINARI A., MOUFKI A., *A new thermomechanical model of cutting applied to turning operations. Part 1, Theory*, Int. J. of Machine Tools and Manufacture, **45**, 166–180, 2005.
27. MOUFKI A., *Contribution à la modélisation de l'usinage par une approche thermo viscoplastique. Application la coupe, orthogonale et oblique* [in French], PhD-Thesis, University of Metz, 1998.
28. BARAUSKAS R., ABRAITIENE A., *Computational analysis of impact of a bullet against the multilayer fabrics in LS-DYNA*, International Journal of Impact Engineering, **34**, 1286–1305, 2007.

29. DEY S., BORVIK T., HOPPERSTAD O.S., LANGSETH M., *On the influence of fracture criterion in projectile impact of steel plates*, Computational Materials Science, **38**, 176–191, 2006.
30. ABUKHSHIM N.A., MATIVENGA P.T., SHEIKH M.A., *Heat generation and temperature prediction in metal cutting: A review and implications for high speed machining*, International Journal of Machine Tools and Manufacture, **46**, 7-8, 782–800, 2006.

Received November 15, 2012; revised version November 25, 2013.
